An Assessment of Regional ICESat-2 Sea-Level Trends

Brett Buzzanga[1,2] , **Eduard Heijkoop[3]** , **Benjamin D. Hamlington[2]** , **R. Steven Nerem[3]** , and **Alex Gardner[2]**

[1]Center for Coastal and Physical Oceanography, Department of Ocean and Earth Sciences, Old Dominion University, Norfolk, VA, USA, [2]Jet Propulsion Laboratory, California Institute of Technology, Pasadena, CA, USA, [3]Colorado Center for Astrodynamics Research, Ann and H. J. Smead Aerospace Engineering Sciences, Cooperative Institute for Research in Environmental Sciences, University of Colorado, Boulder, CO, USA

Abstract Sea-level rise is an important indicator of ongoing climate change and well observed by satellite altimetry. However, observations from conventional altimetry degrade at the coast where regional sea-level changes can deviate from the open-ocean and impact local communities. With the 2018 launch of the laser altimeter onboard ICESat-2, new high-resolution observations of ice, land, and ocean elevations are available. Here we assess the potential benefits of sea level measured by ICESat-2 by comparing to data from Jason-3 and tide gauges. We find good agreement in the linear rates computed from the independent observations, with an absolute average residual of 3.60 ± 0.03 cm yr^{-1} between global ICESat-2 and Jason-3 observations at a 1° posting. The recent La Niña is clearly evident in ICESat-2 observations, as well as small-scale features. By demonstrating the quality of the ICESat-2-measured sea level, we provide support for integrating it into the existing suite of sea-level observations.

Plain Language Summary Sea levels are rising globally due to human induced climate change. However, local sea levels that impact coastal communities often differ from the global increase, sometimes by a factor of 2 or more. Unfortunately, measuring sea level along the coast can be challenging, as radar satellites are primarily designed for the open ocean. Additionally, direct measurements from tide gauge stations are typically spaced far apart, and thus don't adequately represent the full range of changes that occur along the coast. In 2018, NASA launched the ICESat-2 satellite which carries a laser instrument capable of measuring sea level much closer to the coast than existing radar satellites. Here we assess how well ICESat-2 data measures coastal sea level by comparing it to data from the radar satellite Jason-3 and tide gauges measurements. We find good agreement in recent sea-level changes computed from both data sources. Large-scale climate patterns, such as the recent La Niña, as well as small-scale oceanic features like currents are clearly evident in the ICESat-2 data. These results support the idea that ICESat-2 measurements can be integrated into the existing suite of sea-level observations and serve as an additional tool for addressing ongoing sea-level rise.

1. Introduction

The rising trend in global mean sea level is an integrative measure of Earth's warming climate, as melting land-ice and rising water temperatures increase ocean mass and volume (e.g., Church & White, 2011; Frederikse et al., 2020). However, the processes contributing to sea level change interact such that regional sea-level trends and variability can differ substantially from the global mean trend (Figure S1; Hamlington et al., 2020; Holgate & Woodworth, 2004). Coastal communities require accurate information on current and future sea-level change in order to respond to ongoing societal challenges such as enhanced storm surge risk and tidal flooding (e.g., Kirezci et al., 2020).

With multi-decadal records, tide gauges (TGs) are an essential data source for measuring sea-level change (e.g., Mitchum et al., 2010). TGs have revealed invaluable information about Earth's climate and geodetic properties (Cf. Douglas, 1991; Wöppelmann et al., 2006). However, the network of TG stations is heavily biased toward the Northern Hemisphere, especially regarding the longer and quality-controlled records (e.g., Thompson et al., 2016). Additionally, TGs are point sources that capture the sea-level change only at a specific location. TGs therefore undersample dynamic coastal environments, which prevents a full understanding of how sea-level variability propagates toward and along the coast. This shortcoming has

been alleviated in recent decades with spaceborne radar altimeters providing observations of open-ocean changes in sea level with near global coverage (±66°) since 1992 (Fu et al., 1994).

Conventional pulse-limited satellite radar altimeters operate by transmitting microwave pulses toward the Earth and measuring the time delay of the returned echoes to estimate sea surface height (SSH; Chelton et al., 2001). These measurements have significantly advanced our understanding of the global oceans. For example, early missions revealed a highly turbulent, eddy-filled ocean. Contemporary missions provide measurements of the marine geoid upon which spaceborne observation systems rely, as well as sea-level changes informing climate research (Stammer & Cazenave, 2018). However, radar measurements are challenged in the coastal zone (within ~20 km from land) where many of the impacts of sea-level change occur. These challenges stem primarily from the presence of land in the altimeter and radiometer footprint, which decreases the accuracy of the return pulse geolocation and the applied geophysical range corrections, respectively. Similarly, heterogeneity in the radar footprint causes the shape of the waveform to deviate from the shape returned over the open ocean. While the theoretical Brown model (Brown, 1977) is an accurate representation of the open-ocean waveform, it doesn't capture the more complex geometry of coastal waveforms (see Vignudelli et al., 2011 and references therein).

Ongoing advancements in altimeter technologies are addressing these challenges by enabling more precise data returns up to ~300 m of the coast. For example, the SARAL/AltiKa mission's Ka-band (36.5 GHz) radar has improved the radar footprint diameter and sampling frequency, enabling new observations of coastal circulation (Jebri et al., 2016; Pascual et al., 2015) and better measurements of significant wave heights (Verron et al., 2018). Sentinel-3, and soon the NASA/CNES SWOT satellite, utilize synthetic aperture radar altimeters that preserve the phase of the signal return such that the Doppler shift can be exploited to improve retrievals in the coastal zone (Raney, 1998). However, sophisticated retracking algorithms are required for near-shore analysis, with ongoing development for specific coastlines (Cazenave et al., 2019; e.g.,Dinardo et al., 2020).

The wide variety of near-shore geophysical processes calls for a multi-faceted observational approach to measure and understand the spatiotemporal variability of sea level in the coastal zone. Parallel to the progress in coastal altimetry, technological advancements in recent decades have led to the development of spaceborne laser altimeters. ICESat, which operated sporadically between 2003 and 2009, demonstrated potential for high resolution measurements of sea level, but gaps in coverage makes recovering long-term trends non-trivial (Urban et al., 2008). In 2018, NASA launched its Advanced Topographic Laser Altimeter System (ATLAS) aboard ICESat-2, which measures ice, ocean and land surface elevations with a 91-day repeat cycle at the poles and "mapping mode" at lower latitudes. While ICESat-2's primary scientific objectives are not centered around ocean elevation observations, there is nevertheless much potential for ICESat-2 to bring new insight into coastal sea-level changes and its underlying dynamics. An ocean elevation product, ATL12, has been recently derived from the underlying geolocated photons heights (Morison, Dickinson, Hancock, et al., 2020). We focus our analysis exclusively on the first two moments of the SSH distribution, henceforth referring to them as the ATL12 SSH (h) and variance (σ^2), respectively.

In the following, we undertake an initial assessment of the ATL12 product's role in understanding sea-level trends. First, we show overall comparisons between ATL12 data at TGs, and the radar altimeter Jason-3. Next, we present a global view of the sea-level trends estimated from each altimeter. We then discuss the basin-scale oceanographic patterns that are detectable from the ATL12 record. Due to the short length of the ICESat-2 observations (2 years) the level of instrumental signal-to-noise ratio currently precludes an investigation of synoptic and climate variability. Using the current uncertainties, we perform a qualitative error analysis to elucidate the timelines for which climate variability may begin to emerge from the higher-frequency noise. We conclude with a discussion of future opportunities, limitations and avenues for further research.

2. Data and Methods

To assess the performance of the ICESat-2 over the global ocean we acquire several data products for comparison that are publicly available. The ICESat-2 ATL12 Ocean Surface Height Version 3 is provided by the National Snow and Ice Data Center, which is updated quarterly in accordance with the 91 days repeat time

of the satellite (Morison, Dickinson, Hancock, et al., 2020). At the time of writing, we use the latest data that spans October 2018 through November 2020. We retrieve the ocean height (h) variable and variance (h_var) for each along-track beam included in the product (see Morison, Dickinson, Hancock, et al., 2020). From the National Center for Environmental Information at NOAA, we obtain the Jason-3 Geophysical Data Records that cover the ICESat-2 sensing period (Lillibridge et al., 2019). We extract the sea surface height anomaly (SSHa) via the ssha_mle3 variable, which uses the maximum likelihood estimator 3 algorithm for retracking (Thibaut et al., 2010). We explored additional comparisons with the SARAL/ALTIKA data set but found the data during the ICESat-2 period to require specialized processing due to its drifting orbit (Desai, 2013). All data are acquired as along-track products.

In both products, the ocean height variables are provided with geophysical corrections applied. These include tides (ocean and solid-earth) and the inverted barometer effect (Morison, Dickinson, Hancock, et al., 2020). After experimenting with different corrections, we found keeping the corrections applied and subtracting the sea-state bias gave the best results (not shown). The ATL12 ocean elevation data are provided relative to the IGS14 reference ellipsoid and include a geoid estimated from the Earth Gravitational Model 2008. We subtract the geoid at each ATL12 ocean height to yield dynamic ocean topography (DOT; e.g., Kwok & Morison, 2011). This enables a more direct comparison to the Jason-3 SSHa, which reflects SSH relative to the mean sea surface estimated between 1993 and 2009 with the MSS_CNES-CLS11 model and contains the geoid estimate (Picot et al., 2018).

Water pixels are isolated in the ATL12 product using the Global Self-consistent, Hierarchical, High-resolution Geography Database buffered up to 20 km to include near-shore areas such as low-lying land surface, although this still excluded some coastal data (e.g., Figure S2; Morison, Dickinson, Hancock, et al., 2020; Wessel & Smith, 1996). We perform additional masking by excluding samples that do not fall within the ocean polygons available from the Open Street Map project (OpenStreetMap Contributors, 2017). We also excluded data acquired during drag make up operations (Morison, Dickinson, Roberts, & Robbins, 2020). We experimented with removing data acquired during commanded satellite maneuvers performed over the central Pacific ("ocean scans") but found removal of these data reduced the amount of data for trend computations and thus their quality.

To assess ATL12 DOT at the coast, we use data from the global TG network maintained by the Joint Archive for Sea Level (JASL) and accessible through the University of Hawaii Sea Level Center/Joint Institute for Marine and Atmospheric Research. As data from the Research Quality stream is not available after 2019, we use data from the Fast Delivery stream which has records available for most TGs through August 2020 (Caldwell, 2015).

We compute residuals using linear rates calculated between ATL12 ocean heights that overlap in space and time with the other data sources. We do not account for seasonality in the trends, as the limited data prohibit robust recovery of the annual cycle.

For the radar altimetry products, we consider three separate spatial grids with resolution 0.1°, 0.25°, and 0.5°, respectively. In each grid cell, we produce a time series for each sensor (ATL12, Jason-3) by taking an average of the available data. The average of the ATL12 DOT is weighted by the inverse of the variance (σ^2) provided with the product. For all altimetry datasets, we exclude outliers that lie outside the 99th percentile. Only data that overlap in time between sensors are considered. We then difference the linear rates of the ATL12 DOT computed using weighted least squares with linear rates of the Jason-3 computed using ordinary least squares.

Next, we consider TGs in the JASL Fast delivery stream with records that overlap with the ATL12. Within a 0.1°, 0.25°, and 0.5° square centered on each TG we compute an average of the ATL12 data. We treat data that lie beyond ~1 standard deviation of the median as outliers in each ATL12/TG comparison (Iglewicz & Hoaglin, 1993). This additional consideration is motivated by the reduced sample size and enhanced variability of the TG comparisons in the coastal oceans relative to the global oceans. We experimented with additional treatments of outliers, including more flexible median filters, but found negligible differences on the overall results (not shown). We compute the residual between the linear rate for the ATL12 DOT estimated using general least squares and the ordinary least squares linear rate of the TG data. We discard
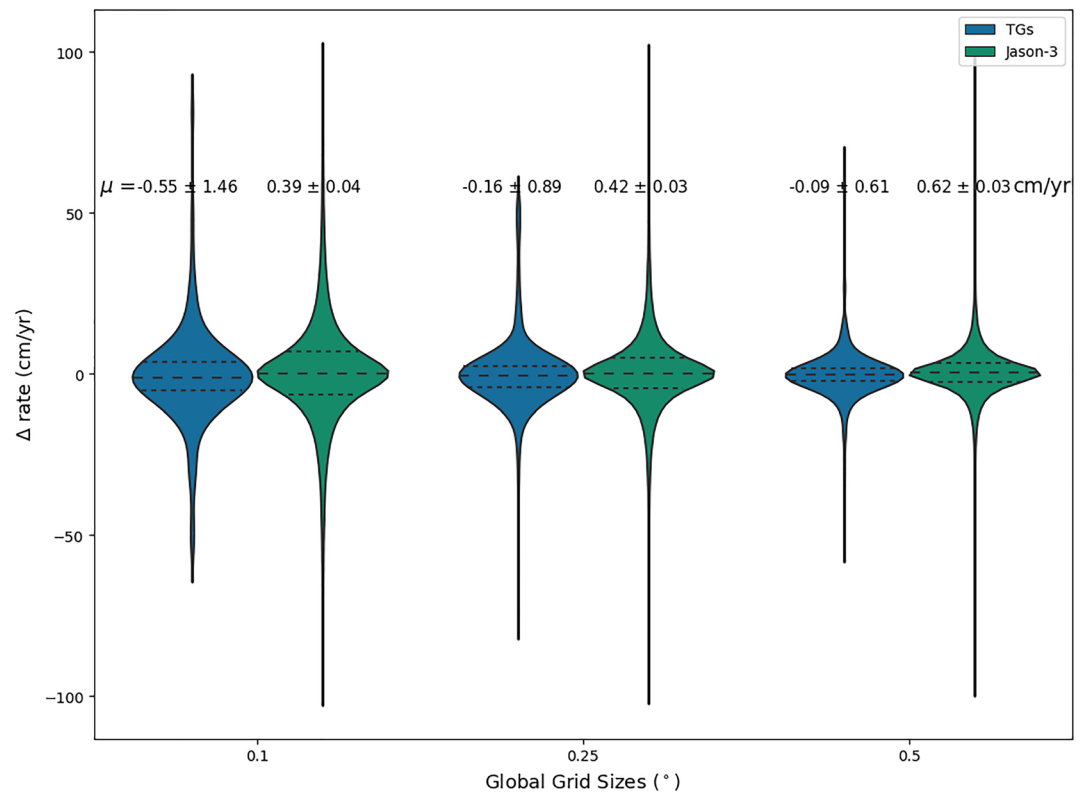
Figure 1. Violin plots combining boxplots and histograms for ICESat-2 comparisons. The median and quartiles are marked as horizontal dashed lines, and the width of the violin shows the smoothed kernel density estimate. The underlying distributions are residuals between ATL12 minus the Joint Archive of Sea Level (JASL) hourly fast delivery records (blue), and ATL12 minus Jason-3 (teal). Mean and standard error are reported for each comparison. ATL, Advanced Topographic Laser.

residuals greater than 100 cm for both TG and Jason-3 comparisons, resulting in 104, 194, and 215 ATL12/TG comparisons for 0.1°, 0.25°, and 0.5°, respectively, and greater than 75,000 for all Jason-3 grid sizes.

3. Results

Figure 1 shows an overview of the linear rate comparisons between the ATL12 DOT, JASL hourly fast delivery TG records and Jason-3 along-track altimetry retrievals. The violins combine a boxplot and histogram, with the median and quartile ranges as horizontal dashed lines, and the kernel density estimate of the distribution on the vertical axis. The mean and standard error are marked for each violin. The size of the grid has a clear effect on the ATL12-TG residuals. The extremes and standard errors are inversely correlated to grid size, as larger samples of ATL12 DOT mitigate the impact of outliers. Note that vertical land motion affecting the TG rate calculations is largely within the noise of the residuals. The effects of gridding are smaller on the ATL12-Jason-3 residuals, as the open-ocean variability is reduced relative to the coastal waters sampled by TGs and sampling sizes are negligibly different.

In Figure 2 we present the ATL12 - JASL TG 0.5° comparison spatially to highlight regional performances. The 0.5° comparison performed markedly better than the smaller grid sizes. There is no obvious global bias to the residuals, and we do not find substantial differences at high latitudes due to orbital convergence near the poles, but some coastlines perform markedly better than others. The Atlantic Coastlines show good agreement, with the exception of a few TGs in high latitudes and the Caribbean Islands. The Pacific residuals are more heterogeneous, with good agreement along the East Asian and Western South American Coasts, but poorer comparisons along Western North America and the Tropical Pacific Islands. The residuals along the Indian and East African Coasts are particularly high, indicating errors in one or both of the data sources along these coasts.
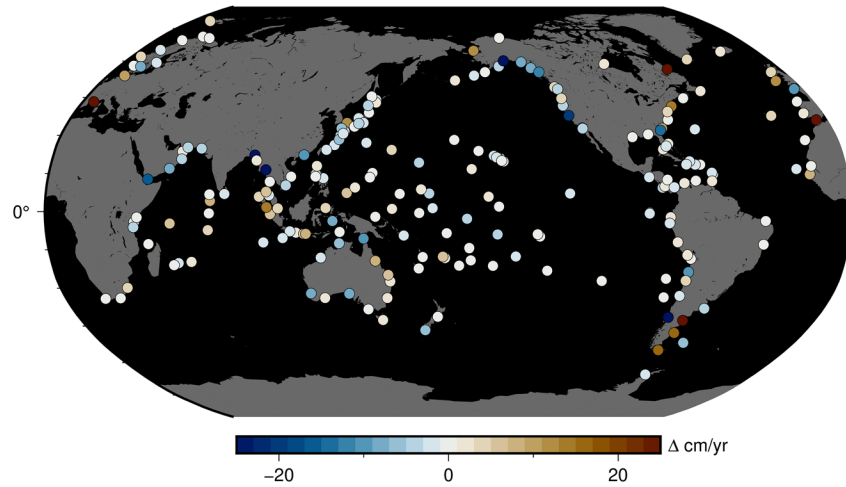
Figure 2. Global comparisons of ATL12 DOT rates in a 0.5° box centered on hourly tide gauge data acquired from the Joint Archive of Sea Level at the University of Hawaii. Data exceeding ~1 standard deviation of the median is discarded in each time series. ATL, Advanced Topographic Laser; DOT, dynamic ocean topography.

However, over the global oceans, there is remarkable agreement between ATL12 DOT and Jason-3 SSHa (Figure 3). Overall, the two data sources have an absolute residual $|\text{DOT} - \text{SSH}|$ mean of 3.60 ± 0.03 cm yr^{-1} with a standard deviation of 5.94 cm yr^{-1}. There are clear basin scale patterns, especially in the equatorial band of the Pacific. Similarly, the Indian Ocean shows excellent agreement, with elevated rates in the central and Northern regions, and negative rates further south. Very similar regional patterns are also visible in both data sources, such as the sea-level fall in the Red Sea, an absence of sea-level change in the Mediterranean Sea, and high rates of rise in the Baltic Sea. A number of localized features are apparent, including the energetic western boundary currents in the North Hemisphere, and the eddy-driven Antarctic Circumpolar Current. Although particularly noisy ICESat-2 tracks appear as roughly N/S streaks in several places (such as the northern coast of Brazil), these typically arise from data outliers in a single orbit and can be isolated and removed with specialized post-processing.

Nevertheless, there is still considerable noise associated with the ATL12 trend estimates. Figure S3 captures the substantial amount of spatiotemporal variability in 1.0° grid cells along the U.S. East Coast. While this variability contains climate signals that manifest as mm-scale SSH changes, the observed cm-m scale variations are mainly imparted by instantaneous oceanic and atmospheric conditions that can be reduced through averaging as the ICESat-2 time-series lengthens.

Figure 4 presents a qualitative estimate of the effects of further ATL12 samples on uncertainty of the estimated trends. Here we consider 0.25°, 0.5°, and 1.0° grid sizes spanning the global oceans. In each grid cell, we construct a single time series $\langle \text{DOT} \rangle$ by averaging N ATL12 DOT samples, weighted by the diagonal covariance matrix $\boldsymbol{Q}$ of ATL12 uncertainty estimates that fall within the same hour:

$$\langle \text{DOT} \rangle = \left(A^T \boldsymbol{Q}^{-1} A \right)^{-1} A^T \boldsymbol{Q} \cdot \text{DOT} \tag{1}$$

where is A is an N x 1 identity matrix. We then average and propagate the covariance estimate of $\langle \text{DOT} \rangle$ using the variance propagation law to result in Q:

$$Q = \left(A^T \boldsymbol{Q}^{-1} A \right)^{-1} + \frac{1}{N} \sum_{i=1}^{N} Q_{ii} \tag{2}$$

Next, we generate a 7 years (~November 2018–November 2025) synthetic time series $\langle \text{DOT} \rangle_S$ and $\boldsymbol{Q}_S$ by bootstrapping with replacement. The synthetic time series for each 0.25°, 0.5°, and 1.0° grid in the global oceans have an experimentally determined semimonthly, monthly, and bimonthly sampling interval,
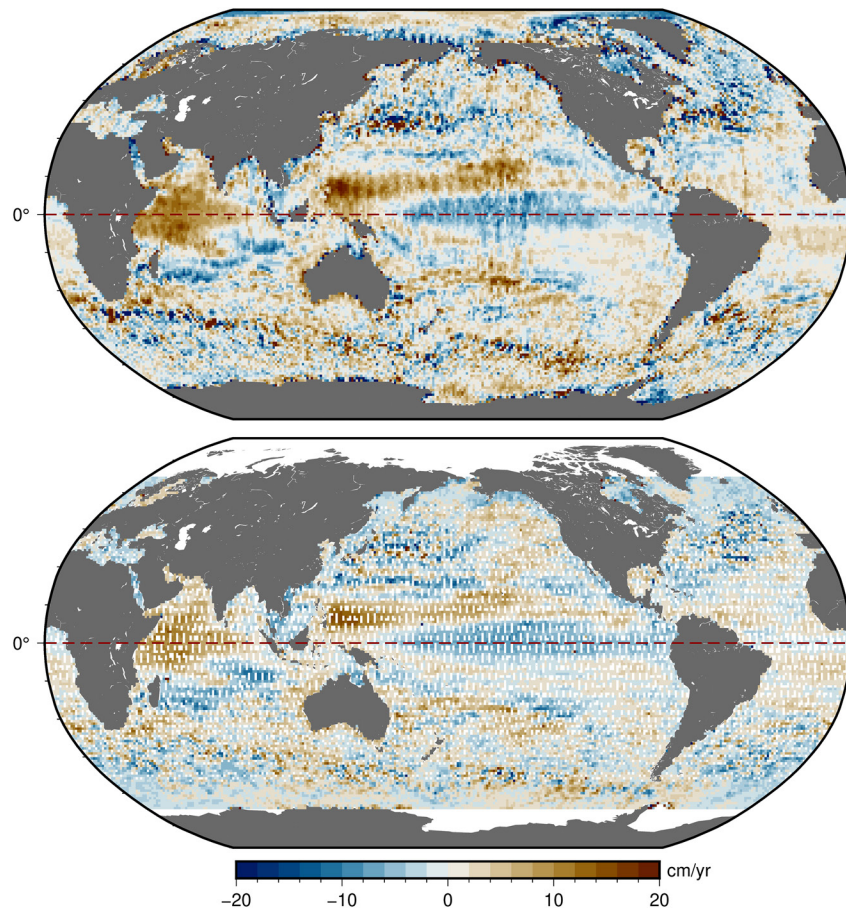
Figure 3. Global sea-level rates in 1° grid computed from ICESat-2 ATL12 (over the period October 2018–November 2020; top) and Jason-3 (October 14, 2018–August 2020; bottom). Individual ATL12 samples are averaged by hour and then subjected to linear least squares fitting. The two data sources have a mean absolute residual of 3.60 ± 0.03 cm yr^{-1} with a standard deviation of 5.94 cm yr^{-1}. ATL, Advanced Topographic Laser.

respectively (Figure S4). Finally, we estimate linear trends for each successive sample in time of $\langle \mathrm{DOT} \rangle_S$, weighted by $\boldsymbol{Q}_S$ (Figure 4).

While not a rigorous accounting, the standard error of the rate estimate improves considerably for all grid sizes. In one sense, these are conservative estimates, given that the temporal correlation of the global sea level trend is not accounted for and will become more apparent as the time series lengthens. However, lower frequency ocean process variability will also further impact the uncertainty estimates as the time series, obfuscating temporal correlations that would otherwise be apparent. Additionally, there are uncertainties in the geophysical corrections such as sea state bias, the calculation of the geoid used to calculate DOT from ocean elevation, and unaccounted for instrumental uncertainties that require elucidation beyond this analysis.

4. Discussion

Despite having a short time-series relative to TG and radar altimeter records, ICESat-2 derived products have already been shown to be important observations for a variety of scientific purposes. For example, Klotz et al., (2020) map individual waves along the ICESat-2 track and infer wave spectra and wind speed. Others have explored wave detection in sea ice (Horvat et al., 2020), inland water monitoring (Ryan et al., 2020; Yuan et al., 2020), and bathymetry detection (Albright & Glennie, 2020; Armon et al., 2020). By demonstrating general agreement between independent data sources (Figure 1), our analysis indicates an important role for ICESat-2 in observing ongoing sea-level change.
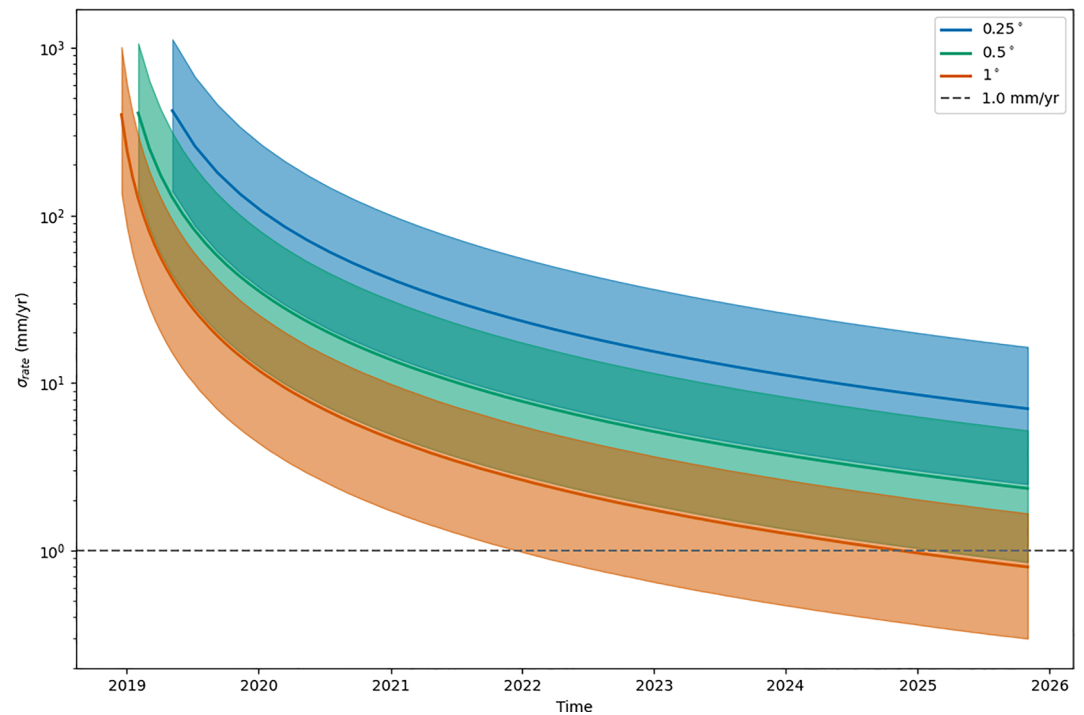
Figure 4. Uncertainty reduction through time of synthetic ATL12 data in 0.25°, 0.5°, and 1.0° grid cells spanning the globe. Synthetic data is created by bootstrapping the averaged ATL12 DOT and variance within each grid cell and propagating the uncertainty. The heavy lines show the median estimate, and the shading indicates the 95% confidence interval for each grid size. ATL, Advanced Topographic Laser; DOT, dynamic ocean topography.

Both along coastlines (Figure 2, Figure S5) and in the open ocean (Figure 3) ICESat-2 observations complement existing measurements by filling in the gaps between TGs and altimeter tracks (Figure S2). The large-scale oceanographic patterns seen in Jason-3 are clearly visible in ATL12 products at much higher resolution (Figure 3). For example, the effects of the 2019 La Niña that dominated tropical Pacific sea-level change during the ICESat-2 sensing period (October 2018 - Present) are clearly present. The enhanced easterly trade winds and associated circulation led to anomalously high sea-level rates near Indonesia and lower rates in the central and eastern Pacific (Figure 3). Also clearly evident are the high rates of sea-level change in much of the Indian Ocean, arising from the anomalous Indian Ocean Dipole event that occurred in late 2019–2020 (Lu & Ren, 2020). Mesoscale eddies are well sampled, and ICESat-2 can contribute to investigations of eddy spatial structure (Chelton et al., 2007) and their role in transporting ocean heat and salinity and kinetic energy (e.g., Dong et al., 2014; Ezer, 2015)

There are still non-negligible uncertainties in the ICESat-2 measurements (Figure 4). However, as with radar-altimeters, the signal-to-noise ratio will increase as the data record lengthens. Moreover, recent work has sought to improve the estimation of sea-state bias from laser altimetry (J. Morison et al., 2018), while ongoing research is targeting the substantial uncertainty caused by large waves (Morison, Dickinson, Hancock, et al., 2020). Additionally, a monthly mean sea-surface product (ATL19) gridded at 0.25° between ±60° and at a 25 km projection at the poles will be released in 2021.

Such improvements will further enhance ICESat-2's role in understanding sea-level change. The excellent agreement with the Jason-3 altimeter data highlights the potential for ICESat-2 to contribute to our existing observations of sea level. Particularly important are coastal and polar oceans, where existing altimetry data is degraded and/or absent (Cf. Figure 2, Figure S6). These historically undersampled regions are important due to the central role of the polar oceans in the climate system (e.g., Fyke et al., 2018) and the socioeconomic impact of sea-level change at the coast (e.g., Kirezci et al., 2020). Moreover, sea-level variability is often greater along the coast than in the open ocean, due primarily to the impact of bathymetry on dynamic processes (e.g., Hughes et al., 2019).

ICESat-2 offers a new observational tool for understanding coastal sea-level propagation and its physical drivers. No individual sensor by itself can provide a complete sampling of the numerous processes at the coast (Woodworth et al., 2019), necessitating a suite of observational tools. This suite will continue to grow due to the commitment by ESA to support Copernicus through 2030, and the upcoming NASA SWOT and NISAR missions. These instruments will continue to advance our understanding of sea level drivers in the coming years and decade. As tidal flooding and event-driven surges continue to impact coastal communities, this is societally relevant information crucial for fostering mitigation and adaptation to ongoing climate change.

Data Availability Statement

All data used in this study is freely available. ATL12 ICESat-2 data are available at the NSIDC (J. H. Morison, 2020; https://nsidc.org/data/ATL12/versions/3). Jason-3 data are available from NCEI (Lillibridge, 2019; https://www.ncei.noaa.gov/products/jason-satellite-products). Tide gauge data are available from the University of Hawaii Sea Level Center (Caldwell, 2015; https://uhslc.soest.hawaii.edu/datainfo). Water polygons for masking are available from Open Street Maps (OSM 2017; https://osmdata.openstreetmap.de/data/water-polygons.html).

References

Albright, A., & Glennie, C. (2020). Nearshore bathymetry from fusion of Sentinel-2 and ICESat-2 Observations. *IEEE Geoscience and Remote Sensing Letters*, 1–5. https://doi.org/10.1109/LGRS.2020.2987778

Armon, M., Dente, E., Shmilovitz, Y., Mushkin, A., Cohen, T. J., Morin, E., & Enzel, Y. (2020). Determining bathymetry of shallow and ephemeral desert lakes using satellite imagery and altimetry. *Geophysical Research Letters*, 47. https://doi.org/10.1029/2020gl087367

Brown, G. (1977). The average impulse response of a rough surface and its applications. *IEEE Journal of Oceanic Engineering*, 2(1), 67–74. https://doi.org/10.1109/joe.1977.1145328

Caldwell, P., Merrifield, M., & Thompson, P. (2015). *Sea level measured by tide gauges from global oceans–The Joint Archive for Sea Level holdings (NCEI Accession 0019568), Version 5.5*. NOAA National Centers for Environmental Information, Dataset. http://doi.org/10.7289/V5V40S7W

Cazenave, A. A., Gouzenes, Y., Leger, F., Birol, F., Passaro, M., Legeais, J., & Benveniste, J. (2019). *Coastal sea level rise from reprocessed altimetry differs from offshore*. AGU Fall Meeting Abstracts.

Chelton, D. B., Ries, J. C., Haines, B. J., Fu, L.-L., and Callahan, P. S. (2001). Chapter 1 Satellite Altimetry. *International Geophysics*, 69, 1–131. https://doi.org/10.1016/s0074-6142(01)80146-7

Chelton, D. B., Schlax, M. G., Samelson, R. M., & de Szoeke, R. A. (2007). Global observations of large oceanic eddies. *Geophysical Research Letters*, 34. https://doi.org/10.1029/2007gl030812

Church, J. A., & White, N. J. (2011). Sea-Level rise from the late 19th to the early 21st century. *Surveys in Geophysics*, 32, 585–602. https://doi.org/10.1007/s10712-011-9119-1

Desai, S. (2013). *ALTIKA_SARAL_L2_OST_XOGDR. Ver. 1*. PO.DAAC. https://doi.org/10.5067/AKASA-XOGD1

Dinardo, S., Fenoglio-Marc, L., Becker, M., Scharroo, R., Fernandes, M. J., Staneva, J., et al. (2020). A RIP-based SAR retracker and its application in North East Atlantic with Sentinel-3. *Advances in Space Research*. https://doi.org/10.1016/j.asr.2020.06.004

Dong, C., McWilliams, J. C., Liu, Y., & Chen, D. (2014). Global heat and salt transports by eddy movement. *Nature Communications*, 5, 3294. https://doi.org/10.1038/ncomms4294

Douglas, B. C. (1991). Global sea level rise. *Journal of Geophysical Research*, 96, 6981–6992. https://doi.org/10.1029/91jc00064

Ezer, T. (2015). Detecting changes in the transport of the Gulf Stream and the Atlantic overturning circulation from coastal sea level data: The extreme decline in 2009–2010 and estimated variations for 1935–2012. *Global and Planetary Change*, 129, 23–36. https://doi.org/10.1016/j.gloplacha.2015.03.002

Frederikse, T., Landerer, F., Caron, L., Adhikari, S., Parkes, D., Humphrey, V. W., et al. (2020). The causes of sea-level rise since 1900. *Nature*, 584, 393–397. https://doi.org/10.1038/s41586-020-2591-3

Fu, L.-L., Christensen, E. J., Yamarone, C. A., Jr, Lefebvre, M., Ménard, Y., Dorrer, M., & Escudier, P. (1994). TOPEX/POSEIDON mission overview. *Journal of Geophysical Research*, 99, 24369–24381. https://doi.org/10.1029/94jc01761

Fyke, J., Sergienko, O., Löfverström, M., Price, S., & Lenaerts, J. T. M. (2018). An overview of interactions and feedbacks between ice sheets and the earth system. *Reviews of Geophysics*, 56, 361–408. https://doi.org/10.1029/2018rg000600

Hamlington, B. D., Gardner, A. S., Ivins, E., Lenaerts, J. T. M., Reager, J. T., Trossman, D. S., et al. (2020). Understanding of contemporary regional sea-level change and the implications for the future. *Reviews of Geophysics*, 58. https://doi.org/10.1029/2019RG000672

Holgate, S. J., & Woodworth, P. L. (2004). Evidence for enhanced coastal sea level rise during the 1990s. *Geophysical Research Letters*, 31. https://doi.org/10.1029/2004gl019626

Horvat, C., Blanchard-Wrigglesworth, E., & Petty, A. (2020). Observing waves in sea ice with ICESat-2. *Geophysical Research Letters*, 47. https://doi.org/10.1029/2020gl087629

Hughes, C. W., Fukumori, I., Griffies, S. M., Huthnance, J. M., Minobe, S., Spence, P., et al. (2019). Sea level and the role of coastal trapped waves in mediating the influence of the open ocean on the coast. *Surveys in Geophysics*, 40, 1467–1492. https://doi.org/10.1007/s10712-019-09535-x

Iglewicz, B., & Hoaglin, D. C. (1993). *How to detect and handle outliers?* Asq Press.

Jebri, F., Birol, F., Zakardjian, B., Bouffard, J., & Sammari, C. (2016). Exploiting coastal altimetry to improve the surface circulation scheme over the central Mediterranean Sea. *Journal of Geophysical Research: Oceans*, 121, 4888–4909. https://doi.org/10.1002/2016jc011961

Kirezci, E., Young, I. R., Ranasinghe, R., Muis, S., Nicholls, R. J., Lincke, D., & Hinkel, J. (2020). Projections of global-scale extreme sea levels and resulting episodic coastal flooding over the 21st Century. *Scientific Reports*, *10*, 11629. https://doi.org/10.1038/s41598-020-67736-6

Klotz, B. W., Neuenschwander, A., & Magruder, L. A. (2020). High-resolution ocean wave and wind characteristics determined by the ICESat-2 land surface algorithm. *Geophysical Research Letters*, *47*. https://doi.org/10.1029/2019gl085907

Kwok, R., & Morison, J. (2011). Dynamic topography of the ice-covered Arctic Ocean from ICESat. *Geophysical Research Letters*, *38*. https://doi.org/10.1029/2010gl046063

Lillibridge, J.U.D.O. of S.D.P., and Distribution. (2019). Jason-3 level-2 operational, interim and final geophysical data records (X-GDR). NOAA National Centers for Environmental Information. 2016 to present (NCEI Accession 0122595) https://accession.nodc.noaa.gov/0122595.SSH_subset

Lu, B., & Ren, H.-L. (2020). What caused the extreme Indian Ocean dipole event in 2019? *Geophysical Research Letters*, *47*. https://doi.org/10.1029/2020gl087768

Mitchum, G. T., Nerem, R. S., Merrifield, M. A., & Gehrels, W. R. (2010). Modern sea-level-change estimates. In J. A. Church, P. L. Woodworth, T. Aarup, & W. S. Wilson (Eds.), Understanding Sea-Level Rise and Variability (pp. 122–142). https://doi.org/10.1002/9781444323276.ch5

Morison, J., Kwok, R., Dickinson, S., Morison, D., Peralta-Ferriz, C., & Andersen, R. (2018). Sea state bias of ICESat in the subarctic seas. *IEEE Geoscience and Remote Sensing Letters*, *15*, 1144–1148. https://doi.org/10.1109/lgrs.2018.2834362

Morison, J. H. (2020). *ATLAS/ICESat-2 L3A Ocean Surface Height, version 3*. NASA National Snow and Ice Data Center DAAC.

Morison, J. H., Dickinson, S., Hancock, D., Roberts, L., & Robbins, J. (2020). ICESat-2 ATL12 release 4: Ocean altimetry from 10-m to global scales.

Morison, J. H., Dickinson, S., Roberts, D. H. L., & Robbins, J. (2020). ICE, cloud, and land elevation satellite-2 (ICESat-2) ATL12 Ocean Surface height release 003 application notes and known issues.

Open Street map Contributors (OSM). (2017). Planet.osm retrieved from https://planet.osm.org

Pascual, A., Lana, A., Troupin, C., Ruiz, S., Faugère, Y., Escudier, R., & Tintoré, J. (2015). Assessing SARAL/AltiKa data in the coastal zone: Comparisons with HF radar observations. *Marine Geodesy*, *38*, 260–276. https://doi.org/10.1080/01490419.2015.1019656

Picot, N., Marechal, C., Couhert, A., Desai, S., Scharroo, R., & Egido, A. (2018). *Jason-3 products handbook*. Jason-3 Mission Requirements Documents.

Raney, R. K. (1998). The delay/Doppler radar altimeter. *IEEE Transactions on Geoscience and Remote Sensing*, *36*, 1578–1588. https://doi.org/10.1109/36.718861

Ryan, J. C., Smith, L. C., Cooley, S. W., Pitcher, L. H., & Pavelsky, T. M. (2020). Global characterization of inland water reservoirs using ICESat-2 altimetry and climate reanalysis. *Geophysical Research Letters*, *47*. https://doi.org/10.1029/2020gl088543

Stammer, D., & Cazenave, A. (2018). *Satellite Altimetry Over Oceans and Land Surfaces*. CRC Press.

Thibaut, P., Poisson, J. C., Bronner, E., & Picot, N. (2010). Relative performance of the MLE3 and MLE4 retracking algorithms on Jason-2 altimeter waveforms. *Marine Geodesy*, *33*, 317–335. https://doi.org/10.1080/01490419.2010.491033

Thompson, P. R., Hamlington, B. D., Landerer, F. W., & Adhikari, S. (2016). Are long tide gauge records in the wrong place to measure global mean sea level rise? *Geophysical Research Letters*, *43*, 10403–10411. https://doi.org/10.1002/2016gl070552

Urban, T. J., Schutz, B. E., & Neuenschwander, A. L. (2008). A survey of ICESat coastal altimetry applications: Continental coast, open ocean island, and inland river. *Terrestrial, Atmospheric and Oceanic Sciences*, *19*, 1–19. https://doi.org/10.3319/tao.2008.19.1-2.1(sa)

Verron, J., Bonnefond, P., Aouf, L., Birol, F., Bhowmick, S., Calmant, S., et al. (2018). The benefits of the Ka-Band as evidenced from the SARAL/AltiKa altimetric mission: Scientific applications. *Remote Sensing*, *10*, 163. https://doi.org/10.3390/rs10020163

Vignudelli, S., Kostianoy, A. G., Cipollini, P., & Benveniste, J. (2011). *Coastal altimetry*. Springer Science & Business Media.

Wessel, P., & Smith, W. H. F. (1996). A global, self-consistent, hierarchical, high-resolution shoreline database. *Journal of Geophysical Research*, *101*, 8741–8743. https://doi.org/10.1029/96jb00104

Woodworth, P. L., Melet, A., Marcos, M., Ray, R. D., Wöppelmann, G., Sasaki, Y. N., et al. (2019). Forcing factors affecting sea level changes at the coast. *Surveys in Geophysics*, *40*, 1351–1397. https://doi.org/10.1007/s10712-019-09531-1

Wöppelmann, G., Zerbini, S., & Marcos, M. (2006). Tide gauges and Geodesy: A secular synergy illustrated by three present-day case studies. *Comptes Rendus Geoscience*, *338*, 980–991. https://doi.org/10.1016/j.crte.2006.07.006

Yuan, C., Gong, P., & Bai, Y. (2020). Performance assessment of ICESat-2 laser altimeter data for water-level measurement over lakes and reservoirs in China. *Remote Sensing*, *12*, 770. https://doi.org/10.3390/rs12050770